Reactive oxygen species-based sensing by a single chemoreceptor controls bacterial chemotaxis to copper

Gwennaëlle Louis[1], Pauline Cherry[1], Catherine Michaux[2], Sophie Rahuel-Clermont[3], Marc Dieu[4], Françoise Tilquin[1], Laurens Maertens[1,5], Rob Van Houdt[5], Patricia Renard[4], Eric Perpete[2] and Jean-Yves Matroule[1*]

[1]Research Unit in Biology of Microorganisms (URBM), Department of Biology, Namur Research Institute for Life Sciences (NARILIS), University of Namur, Namur, Belgium.

[2] Laboratoire de Chimie Physique des Biomolécules, Namur Research Institute for Life Sciences (NARILIS) and Namur Institute of Structured Matter (NISM), University of Namur, Rue de Bruxelles, 61, 5000 Namur, Belgium.

[3] Université de Lorraine, CNRS, IMoPA, F-54000 Nancy, France.

[4]MaSUN, Mass Spectrometry Facility, University of Namur, Namur, Belgium.

[5]Microbiology Unit, Interdisciplinary Biosciences, Belgian Nuclear Research Centre (SCK CEN), 2400 Mol, Belgium.

*Corresponding author. Mailing address: Research Unit in Biology of Microorganisms (URBM), 61 Rue de Bruxelles 5000 Namur, Belgium. Phone: (32)81-72-42-45. E-mail: jean-yves.matroule@unamur.be

Abstract

Cell motility is a widespread strategy to maintain the fitness of unicellular and multicellular living organisms. This cellular process relies on a chemoreceptor-dependent sensing of the environment which is converted into an intracellular signal modulating flagellum or cilium rotation. Yet the detailed molecular mechanisms operating at the chemoreceptor sensor domain remain largely unclear.

Here we propose that the negative chemotactic response to toxic copper (Cu) in the free-living bacterium *Caulobacter crescentus* implies an original two-step sensing process based on a Cu binding to the sensor domain of the newly identified chemoreceptor McpR and on the generation of reactive oxygen species (ROS) by Cu. We also provide evidence that the McpR-bound Cu undergoes a redox cycling modulating McpR conformation, which thereby allows a fine and rapid redox tuning of the chemoreceptor activity and the underlying chemotactic response.

36 Cell motility is widely distributed across the three domains of life. For instance, in animals
37 it is involved in fertilization and in neutrophils recruitment to an inflammatory area. It also
38 allows archaea and bacteria to seek nutrients in scarce environments and to flee from toxic
39 compounds while it supports to some extent host tropism in the frame of symbiotic
40 relationships[1].

41 Most of the time, cell motility is driven by chemical gradients and is therefore named
42 chemotaxis. In flagellated bacteria, positive (attraction) and negative (repulsion) chemotactic
43 responses rely on the well characterized CheA-CheY two-component system that modulates
44 flagellar rotation, thereby inducing stochastic direction changes[2]. The activation state of CheA-
45 CheY is controlled by finely tuned cytoplasmic or inner membrane-spanning methyl-accepting
46 chemotaxis proteins (Mcp) monitoring chemical variations in the cytosol or in the periplasm[3].
47 In *Escherichia coli*, the binding of an attractant or a repellent to the Mcp sensor domain is
48 proposed to trigger a conformational change that is propagated via the HAMP (Histidine
49 kinases, Adenyl cyclases, Methyl-accepting proteins and Phosphatases) domain to the Mcp
50 signaling domain[4,5]. Yet, the detailed molecular mechanisms underlying ligand recognition and
51 binding are still largely unexplored.

52 Here we identify and characterize an original integrated copper (Cu) sensing mechanism
53 in the free-living bacterium *Caulobacter crescentus*, which relies on the redox cycling of a Cu
54 ion bound to the sensor domain of the newly-identified McpR. We propose that this Cu redox
55 cycling is fed by Cu-generated reactive oxygen species (ROS) and modulates McpR
56 conformation and activity. This ensures a continuous monitoring of the intracellular Cu status
57 providing a real-time control of the chemotactic response.

58 In a previous study, we described an original bimodal strategy to cope with Cu stress where
59 the flagellated morphotype (swarmer cells) of *C. crescentus* triggers a prompt negative

60 chemotaxis from the Cu source[6]. In the same study, we also showed that a significant
61 intracellular Cu accumulation is a prerequisite to sustain this chemotactic response, suggesting
62 that the sensing of Cu variations when the swarmer (SW) cell swims along the Cu gradient is
63 performed intracellularly.

64 In order to add a subcellular resolution to this Cu accumulation, we measured the Cu
65 content by ICP-OES in SW cell fractionates. In accordance with our previous study[6], Cu
66 exposure led to an important cellular Cu accumulation albeit at a much lesser extent in the
67 cytoplasm than in the periplasm (**Fig. 1A**).

68 The transient maintenance of a high intracellular Cu content in the SW cells may potentially
69 lead to an oxidative stress via the production of superoxide anion ($O_2^{\bullet-}$), hydrogen peroxide
70 (H_2O_2) and hydroxyl radical ($OH^{\bullet}$) (**Extended Data Fig. 1A**). In line with this idea, the relative
71 fluorescence intensity of the ROS sensitive turn-on CellROX Deep Red probe is significantly
72 increased in SW cells exposed to Cu or H_2O_2, the latter being used as a positive control (**Fig.**
73 **1B**). Accordingly, the fluorescence of the cytoplasmic turn-off rxYFP redox biosensor is
74 partially quenched under the same conditions (**Fig. 1C**), mirroring an imbalance of the
75 cytoplasmic GSH-GSSG pool upon oxidative stress (**Extended Data Fig. 1B**). These findings
76 are reinforced by the differential expression of genes involved in oxidative stress response upon
77 Cu stress, including those encoding the catalase KatG (CCNA_03138) and the superoxide
78 dismutases SodA (CCNA_03672) and SodB (CCNA_01855)[7]. Together these data argue for
79 the rapid generation of an oxidative stress in SW cells exposed to Cu.

80 In order to determine whether the Cu-induced ROS play a role in Cu chemotaxis, we
81 envisioned that boosting the aforementioned antioxidant defense system would limit Cu-
82 induced ROS production in SW cells. We ectopically expressed the *sodB* or the *katG* genes in
83 the WT background from the low copy pMR10 plasmid under the control of the strong and

84 constitutive lac promoter. The resulting *sodB*$^+$ and *katG*$^+$ strains prevent the increase of the
85 CellROX Deep Red fluorescence upon Cu exposure, reflecting a potentiation of antioxidant
86 defenses (**Fig. 1D**). In support of this data, the growth of these two optimized *sodB*$^+$ and *katG*$^+$
87 strains is significantly improved under moderate Cu stress (**Fig. 1E**), arguing for a role of $O_2^{\bullet-}$,
88 H_2O_2 and very likely $OH^{\bullet}$ in Cu toxicity.

89 In order to assess the potential role of these ROS in Cu chemotaxis, we took advantage of
90 the aforementioned *sodB*$^+$ and *katG*$^+$ strains, where ROS formation is largely hindered. By
91 using the previously designed Live Chemotaxis Imaging (LCI)[6], we showed that the *sodB*$^+$ and
92 *katG*$^+$ strains are impaired in Cu chemotaxis, at a similar extent to the Δ*cheA1* mutant (**Fig. 1F**,
93 **supplementary information**). Consistent with a role of KatG in H_2O_2 detoxification, the *katG*$^+$
94 strain is also impeded in H_2O_2 chemotaxis (**Extended Data Fig. 2**). These data support a major
95 role of ROS in Cu chemotaxis.

96 To further dissect the detailed mechanisms of Cu sensing, we sought to identify the
97 chemoreceptor involved in Cu chemotaxis. The genome of *C. crescentus* is predicted to encode
98 19 Mcp (named McpA to McpS)[8]. No canonical Cu binding site, including the CXXC motif or
99 the βαββαβ fold[9], could be found by running manual and JPred4-based analyses of the 19 Mcp
100 sequences[10]. Therefore, we proceeded to single in-frame deletions of the 19 *mcp* genes, and
101 their respective chemotactic behavior to Cu was assessed by LCI (**Fig. 2A**). Most of the Δ*mcp*
102 mutants displayed a WT-like behavior with a flight percentage after 25 min varying between
103 15% and 51%. Only Δ*mcpA*, Δ*mcpB* and Δ*mcpR* mutants did not significantly cross the arbitrary
104 threshold of 10% flight, suggesting that Cu chemotaxis might be severely affected in these
105 genetic backgrounds. The Δ*mcpA*, Δ*mcpB* and Δ*mcpR* mutants could be complemented by the
106 expression of an ectopic version of *mcpA*, *mcpB* and *mcpR* on the low copy pMR10 plasmid,
107 respectively, suggesting that they may potentially control Cu chemotaxis (**Extended Data Fig.**

108 **3**). However, McpA and McpB are likely involved in chemotaxis at a more global extent
109 considering (i) the position of the *mcpA* and *mcpB* genes within and in the vicinity of the major
110 chemotaxis cluster, respectively[11], and (ii) the reduced motility halo of the Δ*mcpA* mutant
111 observed in a Cu-free swarming assay (**Extended Data Fig. 4**). In addition, McpB displays the
112 terminal sequence of the CheB/CheR docking site that may be necessary for the adaptive
113 response[12], which will not be considered in this study. Therefore, we aimed at further
114 characterizing the role of McpR in Cu chemotaxis.

115 Owing to the multimeric organization of Mcp clusters in bacteria[13], one may argue that the
116 loss of Cu chemotaxis in the Δ*mcpR* mutant results from a loss of motility and/or a disruption
117 of the general chemotactic machinery. The ability of the Δ*mcpR* mutant to form a motility halo
118 in a Cu-free swarming assay (**Extended Data Fig. 5A**) and to sustain negative chemotaxis to
119 other chemicals, such as zinc (Zn) (**Extended Data Fig. 5B**), refutes this hypothesis. It is also
120 worth mentioning that the loss of Cu chemotaxis in the Δ*mcpR* mutant is not due to a loss of
121 ROS production under Cu stress since the Δ*mcpR* mutant exhibits a similar decrease of the
122 rxYFP fluorescence to the WT strain upon Cu exposure (**Extended Data Fig. 6**).

123 Mcp are able to sense attractants or repellents in a direct or indirect manner[14]. Therefore,
124 we decided to assess by intrinsic fluorescence spectroscopy the direct binding of Cu to purified
125 McpR. When mixed with Cu(I) or Cu(II) at 1:1, 1:10 and 1:100 ratios, the intrinsic McpR
126 fluorescence at 346 nm is quenched in a dose-dependent manner, reflecting a modification of
127 the McpR aromatic residues environment (**Fig. 2B**, see **Extended Data Fig. 7** for full spectra).
128 The dissociation constants (*K*d) of 48 µM +/- 10 µM and 37 µM +/- 9 µM for Cu(I) and Cu(II),
129 respectively, attest to a similar affinity of both ionic forms for McpR. However, the micromolar
130 range of Cu(I) and Cu(II) *K*ds exceeds from several logs the *K*d of well-known
131 cuproproteins[15,16], arguing for a rather low affinity of McpR for Cu. Therefore, one may argue

132 that the high Cu cellular content measured in the Cu-exposed SW cells is necessary to promote
133 a rather labile interaction between McpR and Cu. Interestingly, McpR seems to preferentially
134 bind Cu since Zn, cadmium (Cd), manganese (Mn) and nickel (Ni) had no effect on McpR
135 intrinsic fluorescence (**Extended Data Fig. 8**).

136 The complete loss of Cu-chemotaxis in the *sodB*+ and *katG*+ genetic backgrounds (**Fig.**
137 **1F**) indicates that Cu binding to McpR is solely not sufficient to sustain Cu chemotaxis.
138 Consistent with this idea, we found that H_2O_2 chemotaxis is fully abolished in the Δ*mcpR*
139 mutant, indicative of a role of McpR as a sensor of the oxidative stress (**Fig. 2C**). To dissect the
140 sensing mechanism of Cu-induced ROS by McpR, we assessed by LC/MS the oxidation status
141 of McpR with a particular focus on the sensor domain (residues 1-161) after incubating purified
142 McpR with Cu(II) or Cu(I) +/- H_2O_2 at a 1:100 ratio. Only the Cu(I) + H_2O_2 condition, and to
143 a lesser extent Cu(I), led to a significant oxidation of the McpR sensor domain, and more
144 specifically of the H99 residue. In this particular condition, about 30% of the H99 residues
145 acquired an additional oxygen ion, most likely yielding 2-oxoHis (**Fig. 3A**). In accordance with
146 this observation, the expression of an ectopic $mcpR_{H99A}$ allele in the Δ*mcpR* mutant does not
147 restore its ability to sustain Cu chemotaxis, indicating that H99 is a key residue in McpR Cu
148 chemotaxis (**Fig. 3B**). Noteworthy, H99A mutation does not impede Cd chemotaxis for which
149 McpR is also essential (**Extended Data Fig. 9**), confirming the functionality of $McpR_{H99A}$ and
150 the proper assembly of the chemotactic machinery.

151 Metal catalyzed oxidation (MCO) of histidines via the generation of $OH^{\bullet}$ has been
152 previously described in the *Bacillus subtilis* PerR repressor[17], in yeast SOD1[18], and in amyloid
153 beta (Aβ) peptide[19]. The exact role of this modification remains unknown. In addition, no redox
154 cycling involving 2-oxoHis has been described so far, questioning the relevance of H99
155 oxidation in Cu/ROS sensing. MCO mostly targets the metal-binding residues in a caged

156 process[20], suggesting that H99 may coordinate Cu. H99 oxidation could therefore be a side
157 effect of an $OH^{\bullet}$ generation by one McpR-bound Cu(I) ion in the context of a Fenton-like
158 reaction. To test this hypothesis, we calculated the *K*d values of the $McpR_{H99A}$/Cu(I) and
159 $McpR_{H99A}$/Cu(II) complexes (**Fig. 3C**). H99A mutation triggers a 9.4- and 5.8-fold increase of
160 Cu(I) and Cu(II) *K*d, respectively, relative to McpR, suggesting a key role of H99 in Cu(I) and
161 Cu(II) coordination. The important variability associated with the $McpR_{H99A}$ *K*d values likely
162 reflects a potential instability of this mutant in solution upon Cu(I) and Cu(II) exposure,
163 resulting in the presence of several subpopulations of $McpR_{H99A}$.

164 McpR sequence analysis by the TMHMM 2.0[21] and SignalIP 6.0[22] tools did not reveal any
165 McpR transmembrane domains and signal peptide, respectively, arguing for a cytoplasmic
166 McpR localization and therefore a Cu sensing. The 3D structure prediction of McpR by a fold
167 recognition method (Phyre2[23]) highlights a cysteine (C75) residue in the vicinity of H99 (**Fig.
168 3D**). Cysteine residues often contribute to Cu coordination and the measured 19.8 Å distance
169 in the predicted model is compatible with Cu coordination by C75 and H99 residues[24]. In line
170 with this idea, a Δ*mcpR* mutant expressing an ectopic $mcpR_{C75S}$ allele was unable to trigger Cu
171 chemotaxis (**Fig. 3B**), indicating that C75 also plays a key role in Cu-sensing. As a control, the
172 $McpR_{C75S}$ mutant was still able to flee from H_2O_2 (**Extended Data Fig. 10**), attesting the
173 functionality of the $McpR_{C75S}$ mutant within the chemotaxis machinery. In order to determine
174 whether the loss-of-function of the $McpR_{C75S}$ mutant in Cu chemotaxis resulted from a loss of
175 Cu binding, we calculated the *K*d values of the $McpR_{C75S}$/Cu(I) and $McpR_{C75S}$/Cu(II)
176 complexes. Similar to the H99A mutation, the C75S mutation also impeded Cu(I) binding as
177 attested by a 3.5-fold *K*d increase. Surprisingly, Cu(II) binding to the $McpR_{C75S}$ mutant
178 remained unchanged (**Fig. 3C**), suggesting that C75 is required to coordinate Cu(I) but not
179 Cu(II). Consistent with this observation, H99 oxidation by Cu(I) +/- H_2O_2 is fully abolished in
180 the $McpR_{C75S}$ mutant (**Fig. 3E**). The *K*d values calculated for the $McpR_{C75S}$ and $McpR_{H99A}$

181 mutants are in agreement with the known selective binding of Cu(I) and Cu(II) to cysteine and
182 histidine residues, respectively[24,25].

183 The aforementioned observations led us to the idea that Cu(I) coordination by H99 and
184 C75 is decisive for McpR-mediated Cu chemotaxis. Given the structural changes elicited by
185 the binding of a ligand to a cognate chemoreceptor[26], we envisioned that Cu(I) binding to McpR
186 modulates its conformation. To test this idea, Far-UV circular dichroism (CD) spectroscopy
187 was used to monitor the impact of Cu(I) and Cu(II) on McpR secondary structure. Accordingly,
188 Cu(I) has a more significant impact than Cu(II) on McpR secondary structure (**Fig. 3F**),
189 increasing the α-helix percentage from 23% to 44%.

190 Based on our findings, we propose that Cu excess within the reducing cytoplasm favors
191 Cu(I) coordination to C75 and H99 residues. Cu(I) binding to McpR promotes its
192 conformational change and very likely the modulation of the downstream signaling pathway
193 underlying Cu chemotaxis. In addition, cytoplasmic Cu(I) also catalyzes the production of ROS
194 including $O_2^{\bullet-}$ and H_2O_2. Hydrogen peroxide is then subjected to a local Fenton-like reaction by
195 the C75/H99-coordinated Cu(I), yielding $OH^{\bullet}$ that causes accidental H99 oxidation. This redox
196 reaction oxidizes McpR-bound Cu(I) into McpR-bound Cu(II), resulting in a apo-like
197 conformation. The cytoplasmic reducing conditions likely restore the McpR-bound Cu(I) form
198 and its corresponding conformation in a short period of time. This Cu redox cycling is
199 maintained until the cytoplasmic Cu content reaches a basal level, leading to the loss of Cu
200 binding to McpR. Under this condition, McpR returns to its apo form conformation (**Fig. 4**).

201 Cu sensing within the cytoplasm where the Cu concentration is lower (**Fig. 1A**) and better
202 controlled than in the periplasm would thereby potentiate McpR sensitivity to slight changes of
203 Cu content when the SW cells swim down a Cu gradient (**Fig. 4**).

Author contributions

G.L., P.C., C.M., M.D., E.P., F.T., and L.M. performed the experiments; G.L., P.C., C.M., S.R-C., M.D., L. M, P. R., R.V.H., E.P, and J-Y.M. analyzed the data; G.L. and J-Y.M. initiated and designed the research; G.L. and J-Y.M. wrote the manuscript.

Correspondence

Correspondence and request for materials should be addressed to J-Y.M.

Acknowledgements

We would like to thank Jakob R. Winther for providing the rxYFP construct. We are also grateful to Valérie Charles and Carmela Aprile (CMI laboratory, NISM, UNamur) for the ICP measurements and to Virgile Neyman for technical support during the protein purification. Finally, we would like to acknowledge the URBM members and Johan Wouters (Chemistry Department, UNamur) for fruitful discussions. This work was supported by the University of Namur. G. L. was supported by the Belgian Fund for Industrial and Agricultural Research Associate (FRIA). Catherine Michaux and Eric Perpète thank the Belgian National Fund for Scientific Research for their respective associate and senior research associate positions.

Bibliography

1 Keegstra, J. M., Carrara, F. & Stocker, R. The ecological roles of bacterial chemotaxis. *Nat Rev Microbiol*, doi:10.1038/s41579-022-00709-w (2022).

2 Wadhams, G. H. & Armitage, J. P. Making sense of it all: bacterial chemotaxis. *Nat Rev Mol Cell Biol* **5**, 1024-1037, doi:10.1038/nrm1524 (2004).

3 Yang, W. & Briegel, A. Diversity of Bacterial Chemosensory Arrays. *Trends Microbiol* **28**, 68-80, doi:10.1016/j.tim.2019.08.002 (2020).

4 Parkinson, J. S., Hazelbauer, G. L. & Falke, J. J. Signaling and sensory adaptation in Escherichia coli chemoreceptors: 2015 update. *Trends Microbiol* **23**, 257-266, doi:10.1016/j.tim.2015.03.003 (2015).

5 Samanta, D., Borbat, P. P., Dzikovski, B., Freed, J. H. & Crane, B. R. Bacterial chemoreceptor dynamics correlate with activity state and are coupled over long distances. *Proc Natl Acad Sci U S A* **112**, 2455-2460, doi:10.1073/pnas.1414155112 (2015).

6 Lawaree, E. *et al.* Caulobacter crescentus intrinsic dimorphism provides a prompt bimodal response to copper stress. *Nat Microbiol* **1**, 16098, doi:10.1038/nmicrobiol.2016.98 (2016).

7 Maertens, L., Cherry, P., Tilquin, F., Van Houdt, R. & Matroule, J. Y. Environmental Conditions Modulate the Transcriptomic Response of Both Caulobacter crescentus Morphotypes to Cu Stress. *Microorganisms* **9**, doi:10.3390/microorganisms9061116 (2021).

8 Nierman, W. C. *et al.* Complete genome sequence of Caulobacter crescentus. *Proc Natl Acad Sci U S A* **98**, 4136-4141, doi:10.1073/pnas.061029298 (2001).

9 Lamb, A. L. *et al.* Crystal structure of the copper chaperone for superoxide dismutase. *Nat Struct Biol* **6**, 724-729, doi:10.1038/11489 (1999).

10 Drozdetskiy, A., Cole, C., Procter, J. & Barton, G. J. JPred4: a protein secondary structure prediction server. *Nucleic Acids Res* **43**, W389-394, doi:10.1093/nar/gkv332 (2015).

11 Berne, C. & Brun, Y. V. The Two Chemotaxis Clusters in Caulobacter crescentus Play Different Roles in Chemotaxis and Biofilm Regulation. *J Bacteriol* **201**, doi:10.1128/JB.00071-19 (2019).

12 Barnakov, A. N., Barnakova, L. A. & Hazelbauer, G. L. Comparison in vitro of a high- and a low-abundance chemoreceptor of Escherichia coli: similar kinase activation but different methyl-accepting activities. *J Bacteriol* **180**, 6713-6718, doi:10.1128/JB.180.24.6713-6718.1998 (1998).

13 Briegel, A. *et al.* New insights into bacterial chemoreceptor array structure and assembly from electron cryotomography. *Biochemistry* **53**, 1575-1585, doi:10.1021/bi5000614 (2014).

14 Neumann, S., Hansen, C. H., Wingreen, N. S. & Sourjik, V. Differences in signalling by directly and indirectly binding ligands in bacterial chemotaxis. *EMBO J* **29**, 3484-3495, doi:10.1038/emboj.2010.224 (2010).

15 Xiao, Z. *et al.* Unification of the copper(I) binding affinities of the metallo-chaperones Atx1, Atox1, and related proteins: detection probes and affinity standards. *J Biol Chem* **286**, 11047-11055, doi:10.1074/jbc.M110.213074 (2011).

16 Kahra, D., Kovermann, M. & Wittung-Stafshede, P. The C-Terminus of Human Copper Importer Ctr1 Acts as a Binding Site and Transfers Copper to Atox1. *Biophys J* **110**, 95-102, doi:10.1016/j.bpj.2015.11.016 (2016).

17 Lee, J. W. & Helmann, J. D. The PerR transcription factor senses H2O2 by metal-catalysed histidine oxidation. *Nature* **440**, 363-367, doi:10.1038/nature04537 (2006).
18 Tiwari, M. K., Hagglund, P. M., Moller, I. M., Davies, M. J. & Bjerrum, M. J. Copper ion / H2O2 oxidation of Cu/Zn-Superoxide dismutase: Implications for enzymatic activity and antioxidant action. *Redox Biol* **26**, 101262, doi:10.1016/j.redox.2019.101262 (2019).
19 Ramteke, S. N., Walke, G. R., Joshi, B. N., Rapole, S. & Kulkarni, P. P. Effects of oxidation on redox and cytotoxic properties of copper complex of Abeta1-16 peptide. *Free Radic Res* **48**, 1417-1425, doi:10.3109/10715762.2014.960412 (2014).
20 Stadtman, E. R. Oxidation of free amino acids and amino acid residues in proteins by radiolysis and by metal-catalyzed reactions. *Annu Rev Biochem* **62**, 797-821, doi:10.1146/annurev.bi.62.070193.004053 (1993).
21 Krogh, A., Larsson, B., von Heijne, G. & Sonnhammer, E. L. Predicting transmembrane protein topology with a hidden Markov model: application to complete genomes. *J Mol Biol* **305**, 567-580, doi:10.1006/jmbi.2000.4315 (2001).
22 Teufel, F. *et al.* SignalP 6.0 predicts all five types of signal peptides using protein language models. *Nat Biotechnol*, doi:10.1038/s41587-021-01156-3 (2022).
23 Kelley, L. A., Mezulis, S., Yates, C. M., Wass, M. N. & Sternberg, M. J. The Phyre2 web portal for protein modeling, prediction and analysis. *Nat Protoc* **10**, 845-858, doi:10.1038/nprot.2015.053 (2015).
24 Rubino, J. T. & Franz, K. J. Coordination chemistry of copper proteins: how nature handles a toxic cargo for essential function. *J Inorg Biochem* **107**, 129-143, doi:10.1016/j.jinorgbio.2011.11.024 (2012).
25 Rubino, J. T., Chenkin, M. P., Keller, M., Riggs-Gelasco, P. & Franz, K. J. A comparison of methionine, histidine and cysteine in copper(I)-binding peptides reveals differences relevant to copper uptake by organisms in diverse environments. *Metallomics* **3**, 61-73 (2011).
26 Chervitz, S. A. & Falke, J. J. Molecular mechanism of transmembrane signaling by the aspartate receptor: a model. *Proc Natl Acad Sci U S A* **93**, 2545-2550, doi:10.1073/pnas.93.6.2545 (1996).
27 Poindexter, J. S. The caulobacters: ubiquitous unusual bacteria. *Microbiol Rev* **45**, 123-179, doi:10.1128/mr.45.1.123-179.1981 (1981).
28 Evinger, M. & Agabian, N. Envelope-associated nucleoid from Caulobacter crescentus stalked and swarmer cells. *J Bacteriol* **132**, 294-301, doi:10.1128/jb.132.1.294-301.1977 (1977).
29 Ostergaard, H., Tachibana, C. & Winther, J. R. Monitoring disulfide bond formation in the eukaryotic cytosol. *J Cell Biol* **166**, 337-345, doi:10.1083/jcb.200402120 (2004).
30 Ducret, A., Quardokus, E. M. & Brun, Y. V. MicrobeJ, a tool for high throughput bacterial cell detection and quantitative analysis. *Nat Microbiol* **1**, 16077, doi:10.1038/nmicrobiol.2016.77 (2016).
31 Meier, F. *et al.* Online Parallel Accumulation-Serial Fragmentation (PASEF) with a Novel Trapped Ion Mobility Mass Spectrometer. *Mol Cell Proteomics* **17**, 2534-2545, doi:10.1074/mcp.TIR118.000900 (2018).
32 Zhang, J. *et al.* PEAKS DB: de novo sequencing assisted database search for sensitive and accurate peptide identification. *Mol Cell Proteomics* **11**, M111 010587, doi:10.1074/mcp.M111.010587 (2012).

321

322 # Methods
323

324 **Strains, plasmids and growth conditions**

325 *Caulobacter crescentus* (NA1000 strain) was grown at 30°C in Peptone Yeast Extract (PYE)
326 medium[27] with 5 µg/ml kanamycin, 1 µg/ml chloramphenicol and/or an appropriate
327 concentration of $CuSO_4.5H_2O$ when required. Cultures in exponential phase were used for all
328 experiments. Strains and plasmids are listed in Extended Data Table 1, and the strategies for
329 their construction are available upon request. SW cells isolation was achieved according to [28].

330 **Growth curve measurements**

331 *C. crescentus* exponential phase cultures were diluted in PYE medium to a final $O.D._{660\ nm}$ of
332 0.05 and inoculated in 96-well plates with appropriate $CuSO_4$ concentration when required.
333 Bacteria were then grown for 24 h at 30°C under continuous shaking in an Epoch 2 Microplate
334 Spectrophotometer from BioTek (Santa Clara, CA, USA). The absorbance at $O.D._{660\ nm}$ was
335 measured every 10 min.

336 **Motility assay**

337 *C. crescentus* cultures grown in PYE were diluted to an $O.D._{660\ nm}$ of 0.4 and inoculated with
338 sterile toothpicks on a PYE swarming plates (PYE + 0.25% agar). The plates were incubated at
339 30°C for 3 days, then scanned.

340 **Cellular fractionation and ICP-OES measurements**

341 *C. crescentus* cells were fixed for 20 min in 2% paraformaldehyde at 4°C and then washed three
342 times with an ice-cold wash buffer (10 mM Tris-HCl pH 6.8, 100 µM EDTA). The cells were
343 then incubated with 0.125% zwitterionic detergent. A final centrifugation at 14,500 x g for 15
344 min separated the cytoplasm (and inner membrane fraction) from the periplasm (and outer
345 membrane fraction). The two fractions were incubated overnight with a final concentration of

346 1 M HNO_3 and then analyzed by inductively coupled plasma - optical emission spectrometry
347 (ICP-OES) with an Optima 8000 ICP-OES from PerkinElmer. Cellular Cu concentration were
348 calculated as described in [6].

349 **Oxidative stress measurement with the CellROX Deep Red probe**

350 An exponential phase culture of *C. crescentus* was synchronized to isolate the SW cells. The
351 isolated SW cells were diluted to an OD_{660nm} of 0.2 and incubated for 30 min at 30°C under
352 moderate shaking with 5 µM of CellROX Deep Red probe (ThermoFisher) and appropriate
353 concentrations of $CuSO_4$ or H_2O_2. The bacteria were then washed three times with 20 mM
354 Phosphate Buffer to remove the non-internalized probes. The bacteria were finally transferred
355 into a black bottom 96-wells plate and the fluorescence was monitored at 640/690 nm with a
356 SpectraMax iD3 (Molecular Devices, San Jose, CA, USA).

357 **Oxidative stress measurement with the rxYFP biosensor**

358 The SW cells were isolated from an exponential phase culture overexpressing the rxYFP
359 biosensor[29]. The SW cells were diluted to an OD_{660nm} of 0.4 in a black bottom 96-well plate and
360 mixed with different concentrations of $CuSO_4$ and H_2O_2. The rxYFP fluorescence was then
361 monitored every minute for 20 min at 510/556 nm with a SpectraMax iD3 (Molecular Devices,
362 San Jose, CA, USA).

363 **Live Chemotaxis Imaging**

364 The live chemotaxis imaging (LCI) assay was adapted from[6]. Eight microliters of melted 1.5%
365 agarose H_2O with $CuSO_4$, H_2O_2, $ZnSO_4$ or $CdSO_4$ were loaded into the chamber through the
366 external inlet channels to generate the plug. One hundred and fifty microliters of isolated SW
367 cells were in turn injected into the bacterial chamber through the central inlet channel. Images
368 were collected every min for 25 min in one focal plan (near the liquid surface) in the vicinity
369 of the plug with a Nikon Eclipse Ti2-E inverted microscope equipped with a Nikon 20X/0.5

370 Ph2 objective and with a Hamamatsu C13440 digital camera. Quantitative analysis of the time-
371 lapse images was performed with MicrobeJ[30]. The number of bacteria in a same focal plane
372 was determined at each time point.

373 **Protein expression and purification**

374 A BL21 pET28a-$McpR_{His}$ exponential phase culture was incubated for 3 h under shacking at
375 37°C with 1 mM Isopropyl-β-D-thiogalactopyranoside (IPTG) and then harvested by
376 centrifugation for 30 min at 4,000 x g at 4°C. $McpR_{His}$ induction was verified by 12 % Tricine–
377 sodium dodecyl sulfate–polyacrylamide gel electrophoresis (Tricine–SDS–PAGE), followed
378 by Coomassie Blue staining and by WB using an anti-His antibody (1/5000). In order to purify
379 $McpR_{His}$, the IPTG-induced culture was washed with 0.1 M phosphate buffer (pH 8) and
380 centrifuged for 15 min at 9,000 x g at 4°C. Bacterial cells were lysed at 2.4 kbar using a Cell
381 disruptor (Cell Disruption System – one shot model, Constant). As $McpR_{His}$ was mainly
382 forming inclusion bodies, the pellet fraction was resuspended for 1 h under shaking at 4°C in a
383 0.1 M phosphate buffer (pH 8) containing 6 M guanidine. The solubilized inclusion bodies were
384 centrifuged for 30 min at 9,000 x g at 4 °C. The collected supernatant was dialyzed overnight
385 in a 0.1 M phosphate buffer (pH 8) to remove guanidine.

386 **Fluorescence quenching by Cu and other metal ions**

387 McpR protein concentration was determined (1) by measuring the absorbance of the sample at
388 280 nm with the SpectraMax iD3 or (2) with a Bradford protein assay. 3.58 µM of McpR was
389 incubated with different ratios of $CuSO_4$, Tetrakis(acetonitrile)copper(I) hexafluorophosphate,
390 $ZnSO_4$, $CdSO_4$, $MnSO_4$ and $NiSO_4$ in black bottom 96-wells plates. The fluorescence emission
391 spectra were recorded upon 280 nm excitation with the SpectraMax iD3.

392 **Kd determination**

393 The titration of McpR by Cu(I) or Cu(II) monitored by the protein intrinsic fluorescence
394 intensity quenching was fitted to a single-site hyperbolic model by non-linear regression using
395 the Scidavis 2.7 software to determine the affinity constants. Dissociation constants are reported
396 as the mean value ± standard deviation obtained from a minimum of three independent
397 experiments performed on distinct protein productions.

398 **Identification of McpR oxidation by mass spectrometry**

399 *Protein digestion*

400 McpR samples were treated using Filter-aided sample preparation (FASP) using the following
401 protocol. To first wash the filter, 100 µl of formic acid 1 % were placed in each Millipore
402 Microcon 30 MRCFOR030 Ultracel PL-30 before a 15 min centrifugation at 14,100 x g. For
403 each sample, 40 µg of protein adjusted in 150 µl of 8 M urea buffer (8 M urea in 0.1 M Tris
404 buffer at pH 8.5) were placed individually in a column and centrifuged for 15 min at 14,100 x
405 g. The filtrate was discarded and the columns were washed three times by adding 200 µl of urea
406 buffer followed by a 15 min centrifugation at 14,100 x g. For the reduction step, 100 µl of
407 dithiothreitol (DTT) were added and mixed for 1 min at 400 rpm with a thermomixer before a
408 15 min incubation at 24 °C. The samples were then centrifugated for 15 min at 14,100 x g, the
409 filtrate was discarded and the filter was washed by adding 100 µl of urea buffer before another
410 15 min centrifugation at 14,100 x g. An alkylation step was performed by adding 100 µl of
411 iodoacetamide ((IAA), in urea buffer) in the column and mixing for 1 min at 400 rpm in the
412 dark followed by a 20 min incubation in the dark and a 10 min centrifugation at 14,100 x g. To
413 remove the excess of IAA, 100 µl of urea buffer were added and the samples were centrifuged
414 for 15 min at 14,100 x g. To quench the rest of IAA, 100 µl of DTT were placed on the column,
415 mixed for 1 min at 400 rpm and incubated for 15 min at 24 °C before a 10 min centrifugation
416 at 14,100 x g. To remove the excess of DTT, 100 µl of urea buffer were placed on the column

417 and centrifuged for 15 min at 14,100 x g. The filtrate was discarded and the column was washed
418 three times by adding 100 µl of 50 mM sodium bicarbonate buffer ((ABC), in ultrapure water)
419 followed by a 10 min centrifugation at 14,100 x g. The remaining 100 µl were kept at the bottom
420 of the column to avoid any evaporation in the column. The digestion process was performed by
421 adding 80 µl of mass spectrometry grade trypsin (1/50 in ABC buffer) in the column and mixed
422 for 1 min at 400 rpm followed by an overnight incubation at 24°C in a water saturated
423 environment. The Microcon columns were placed in a 1.5 ml LoBind tube and centrifuged for
424 10 min at 14,100 x g. Fourty µl of ABC buffer were placed on the column before a 10 min
425 centrifugation at 14,100 x g. Ten % Trifluoroacetic acid (TFA) in ultrapure water were added
426 into the LoBind Tube to obtain 0.2 % TFA. The samples were dried in a SpeedVac up to 20 µl
427 and transferred into an injection vial.

428 *Mass spectrometry*

429 The digest was analyzed using nano-LC-ESI-MS/MS tims TOF Pro (Bruker, Billerica, MA,
430 USA) coupled with an UHPLC nanoElute (Bruker).

431 Peptides were separated by nanoUHPLC (nanoElute, Bruker) on a 75 µm ID, 25 cm C18
432 column with integrated CaptiveSpray insert (Aurora, ionopticks, Melbourne) at a flow rate of
433 400 nl/min, at 50°C. LC mobile phases A was water with 0.1% formic acid (v/v) and B ACN
434 with 0.1% formic acid (v/v). Samples were loaded directly on the analytical column at a
435 constant pressure of 800 bar. The digest (1 µl) was injected, and the organic content of the
436 mobile phase was increased linearly from 2% B to 15 % in 36 min, from 15 % B to 25% in 19
437 min, from 25% B to 37 % in 5 min and from 37% B to 95% in 5 min. Data acquisition on the
438 tims TOF Pro was performed using Hystar 5.1 and timsControl 2.0. tims TOF Pro data were
439 acquired using 100 ms TIMS accumulation time, mobility (1/K0) range from 0.6 to 1.6 Vs/cm².
440 Mass-spectrometric analysis were carried out using the parallel accumulation serial

441 fragmentation (PASEF) (1) acquisition method. One MS spectra followed by ten PASEF
442 MSMS spectra per total cycle of 1.1 s.

443 Data analysis was performed using PEAKS Studio X Pro with ion mobility module
444 (Bioinformatics Solutions Inc., Waterloo, ON). Protein identifications were conducted using
445 PEAKS search engine with 15 ppm as parent mass error tolerance and 0.05 Da as fragment
446 mass error tolerance. Carbamidomethylation was allowed as fixed modification, oxidation of
447 methionine, histidine, tryptophan and acetylation (N-term) as variable modification. Enzyme
448 specificity was set to trypsin, and the maximum number of missed cleavages per peptide was
449 set at three. The peak lists were searched against the *E. coli*-K12 (11002 sequences) and
450 *Caulobacter* NA1000 (3863 sequences) from UNIREF 100. Peptide spectrum matches and
451 protein identifications were normalized to less than 1.0% false discovery rate.

452 The identification results were processed with the PTM profile tool from PEAKS, which
453 provides quantitative information of modified peptides compared with unmodified peptides for
454 the modification sites of the protein across all MS samples[31,32].

455 **Circular dichroism**

456 8.95 μM of McpR was incubated with different $CuSO_4$ and Tetrakis(acetonitrile)copper(I)
457 hexafluorophosphate concentrations. Measurements were performed with a MOS-500
458 spectropolarimeter in the far-UV region (190-260 nm), using a 1 mm pathlength cell. Four scans
459 were averaged and base lines were subtracted. Secondary structure analyses were performed on
460 the circular dichroism data with the BeStSel server.

461

462

Figure 1

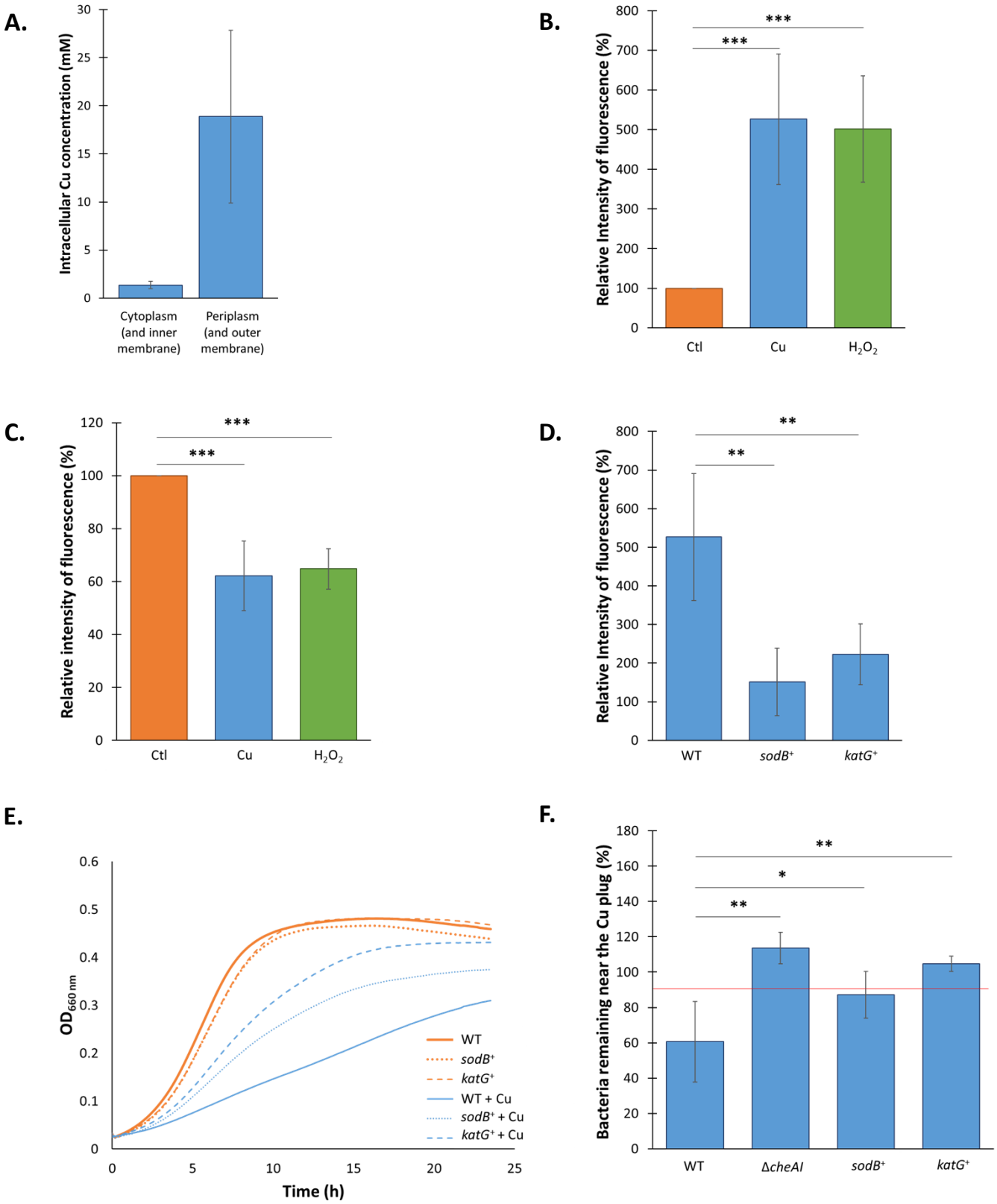
A.
Intracellular Cu concentration (mM)
30
25
20
15
10
5
0
Cytoplasm (and inner membrane)
Periplasm (and outer membrane)
B.
Relative Intensity of fluorescence (%)
800
700
600
500
400
300
200
100
0
***
***
Ctl
Cu
H2O2
C.
Relative intensity of fluorescence (%)
120
100
80
60
40
20
0
***
***
Ctl
Cu
H2O2
D.
Relative Intensity of fluorescence (%)
800
700
600
500
400
300
200
100
0
**
**
WT
sodB+
katG+
E.
OD660 nm
0.6
0.5
0.4
0.3
0.2
0.1
0
0
5
10
15
20
25
Time (h)
WT
sodB+
katG+
WT + Cu
sodB+ + Cu
katG+ + Cu
F.
Bacteria remaining near the Cu plug (%)
180
160
140
120
100
80
60
40
20
0
**
*
**
WT
ΔcheAI
sodB+
katG+

Figure 1: Cu-induced ROS sustain Cu chemotaxis. A. Intracellular Cu concentration in the cytoplasm (and inner membrane fraction) and in the periplasm (and outer membrane fraction) in SW cells exposed to 175 µM Cu for 5 min. **B.** Relative fluorescence intensity of SW cells incubated with 5 µM CellROX Deep Red probe and exposed to 175 µM Cu or 400 µM H_2O_2. **C.** Relative fluorescence intensity of SW cells expressing the rxYFP biosensor and exposed to 175 µM Cu or 400 µM H_2O_2 for 20 min. **D.** Relative fluorescence intensity of WT SW cells and SW cells overexpressing SodB (*sodB*$^+$) and KatG (*katG*$^+$) incubated with 5 µM CellROX Deep Red probe and exposed to 175 µM Cu. **E.** Growth profiles at $OD_{660\ nm}$ of WT, *sodB*$^+$ and *katG*$^+$ strains in PYE (orange) and exposed to 175 µM Cu (blue). **F.** Percentage of WT, Δ*cheAI*, *sodB*$^+$ and *katG*$^+$ SW cells in the vicinity of the Cu plug after 25 min. An arbitrary threshold of 10% flight (corresponding to 90% of cells remaining in the vicinity of the Cu plug) is indicated in red. Mean +/- s.d., at least 3 biological replicates. *p-values* were calculated using an ANOVA when appropriate (* $p < 0.05$, ** $p < 0.01$, *** $p < 0.001$).

Figure 2

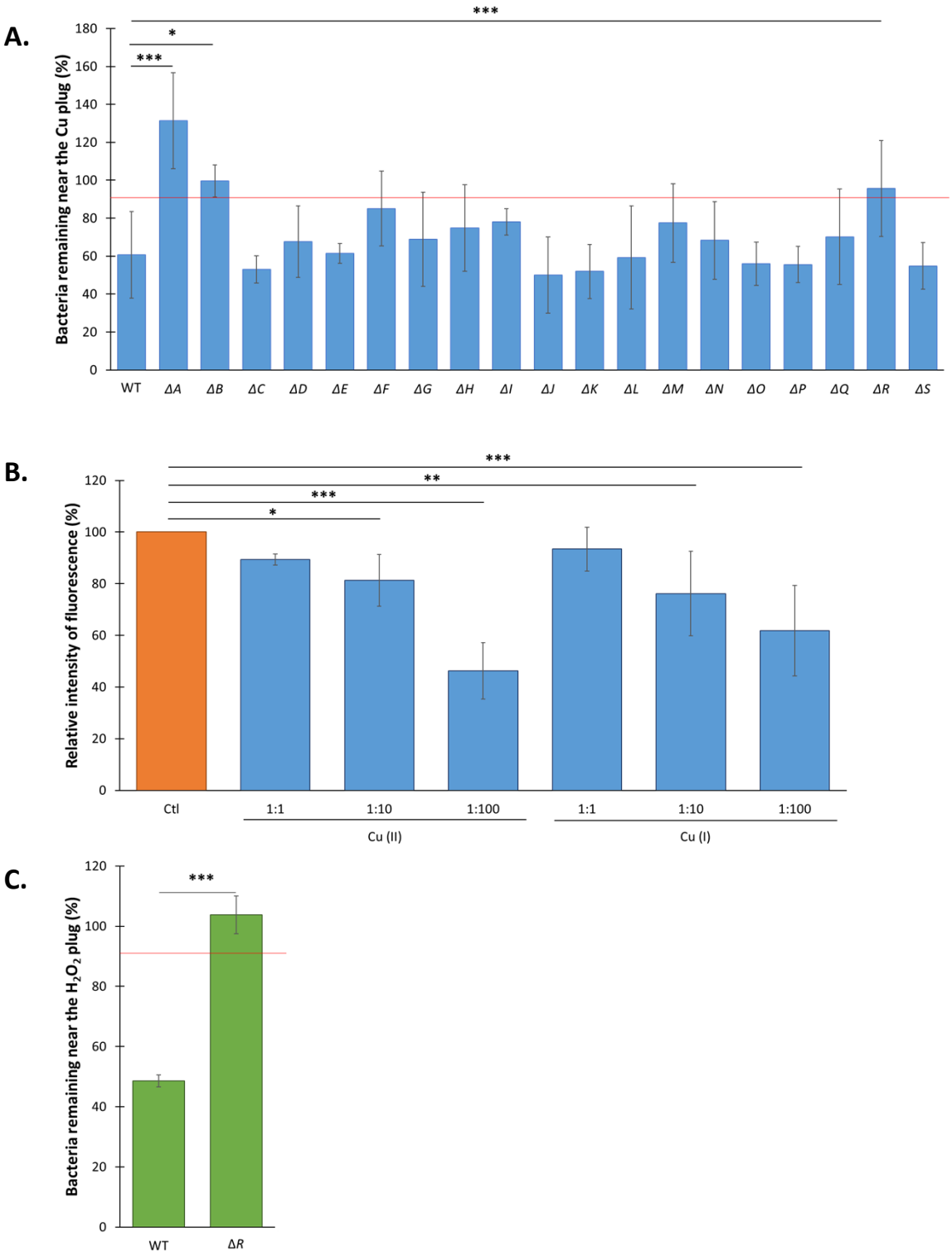
A.
Bacteria remaining near the Cu plug (%)
180
160
140
120
100
80
60
40
20
0
***
*
***
WT
ΔA
ΔB
ΔC
ΔD
ΔE
ΔF
ΔG
ΔH
ΔI
ΔJ
ΔK
ΔL
ΔM
ΔN
ΔO
ΔP
ΔQ
ΔR
ΔS
B.
Relative intensity of fluorescence (%)
120
100
80
60
40
20
0
***
**
***
*
Ctl
1:1
1:10
1:100
1:1
1:10
1:100
Cu (II)
Cu (I)
C.
Bacteria remaining near the H_2O_2 plug (%)
120
100
80
60
40
20
0
***
WT
ΔR

Figure 2: McpR is involved in Cu chemotaxis and Cu binding. A. Percentage of WT and Δ*mcp (mcpA* to *mcpS)* SW cells remaining in the vicinity of the Cu plug after 25 min. An arbitrary threshold of 10% flight (corresponding to 90% of cells remaining in the vicinity of the Cu plug) is indicated in red. **B.** Relative intrinsic fluorescence intensity of purified McpR (3.58 μM) incubated with Cu(II) and Cu(I) at 1:1, 1:10 and 1:100 ratios. **C.** Percentage of WT and Δ*mcpR* SW cells remaining in the vicinity of the H_2O_2 plug after 25 min. An arbitrary threshold of 10% flight (corresponding to 90% of cells remaining in the vicinity of the H_2O_2 plug) is indicated in red. Mean +/- s.d., at least 3 biological replicates. *p-values* were calculated using an ANOVA when appropriate (* $p < 0.05$, ** $p < 0.01$, *** $p < 0.001$).

Figure 3

A.

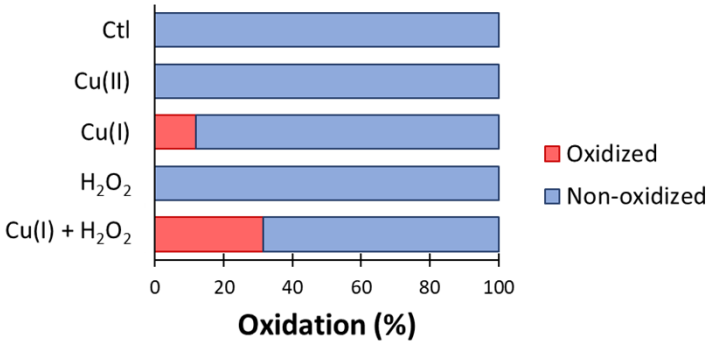

B.

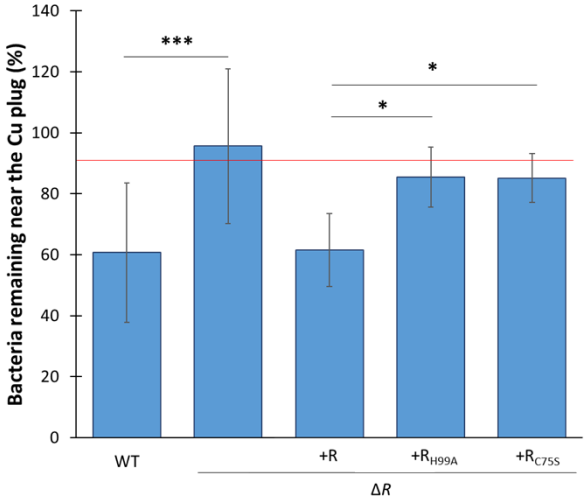

C.

	Cu(I)	Cu(II)
	Kd (µM)	*Kd* (µM)
McpR	48 ± 10	37 ± 9
$McpR_{H99A}$	451 ± 205	213 ± 140
$McpR_{C75S}$	168 ± 83	46 ± 23

D.

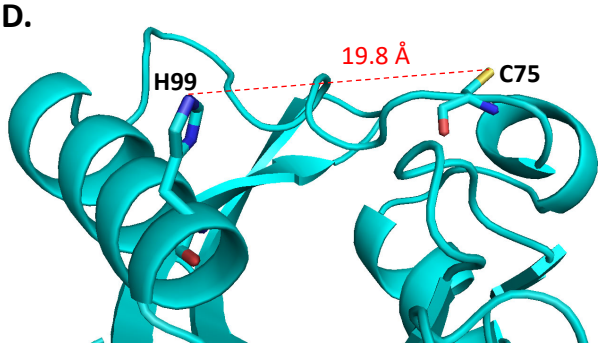

E.

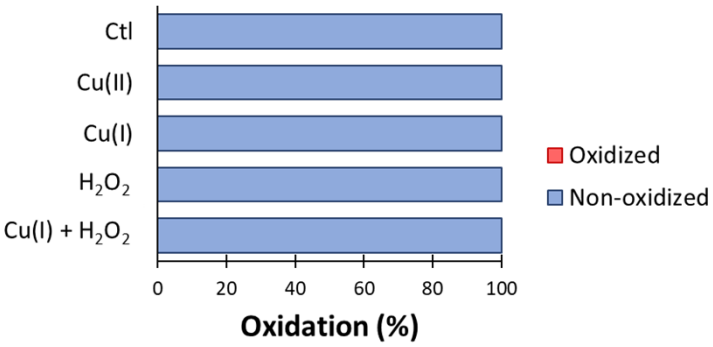

F.

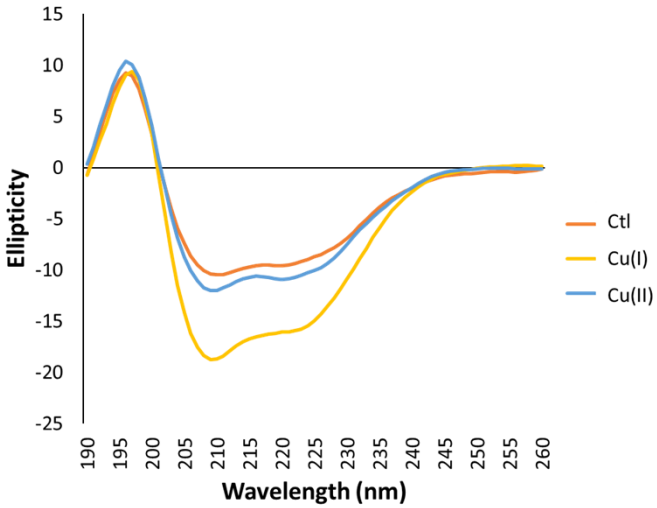

Figure 3: Cu cycling modulates its coordination by the H99 and C75 residues. A. Percentage of oxidation of the H99 residue from purified McpR incubated with Cu(II), Cu(I), H_2O_2 and Cu(I)+H_2O_2 at a 1:100 ratio. **B.** Percentage of SW cells with a WT, Δ*mcpR* and Δ*mcpR* overexpressing McpR, $McpR_{H99A}$ or $McpR_{C75S}$ background remaining in the vicinity of the Cu plug after 25 min. An arbitrary threshold of 10% flight (corresponding to 90% of cells remaining in the vicinity of the Cu plug) is indicated in red. Mean +/- s.d., at least 3 biological replicates. *p-values* were calculated using an ANOVA (* $p < 0.05$, ** $p < 0.01$, *** $p < 0.001$). **C.** Measure, by intrinsic fluorescence, of the *K*d values of purified McpR, $McpR_{H99A}$ and $McpR_{C75S}$ (1.79 µM) incubated with 0 to 500 µM Cu(I) and Cu(II). Mean +/- s.d. **D.** 3D structure prediction of the sensor domain of McpR by Phyre 2. H99 and C75 residues are highlighted. The distance was measured with PyMOL viewer **E.** Percentage of oxidation of the H99 residue from purified $McpR_{C75S}$ incubated Cu(II), Cu(I), H_2O_2 and Cu(I)+H_2O_2 at a 1:100 ratio. **F.** Circular Dichroism spectra of purified McpR (8.95 µM) incubated with Cu(I) and Cu(II) at a 1:100 ratio.

Figure 4

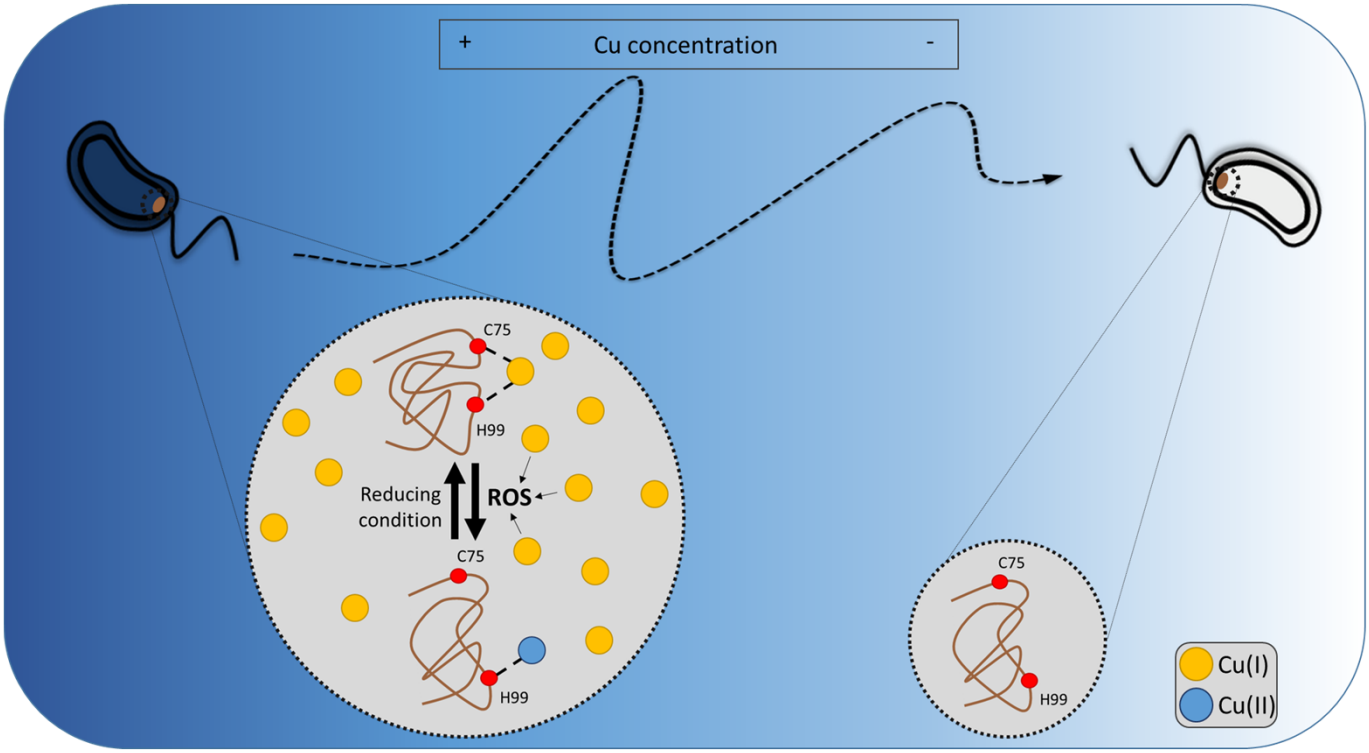
+
Cu concentration
-
C75
H99
Reducing
condition
ROS
C75
H99
C75
H99
Cu(I)
Cu(II)

Figure 4: Hypothetical model of Cu sensing by McpR. SW cell exposure to Cu increases the cytoplasmic Cu concentration, leading to the generation of ROS (left). In addition, high cytoplasmic Cu content promotes Cu(I) coordination by the C75 and H99 residues within the cytoplasmic McpR, triggering a conformational change of the chemoreceptor and activating the downstream chemotaxis signaling pathway. The coordinated Cu(I) is rapidly oxidized into Cu(II) by Cu-generated ROS, thereby disrupting the Cu binding to C75 and reverting McpR conformation to an apo form-like conformation. Owing to the reducing cytoplasmic conditions, H99-coordinated Cu(II) is rapidly reduced to Cu(I) by an unknown cytoplasmic reducer, restoring the Cu(I)-bound conformation. This redox Cu cycling is maintained along the extracellular Cu gradient until the SW cell reaches a Cu-poor environment (right). Under these conditions, the cytoplasmic Cu concentration together with the ROS level will return to their basal level and the labile Cu binding to McpR will be hindered, resulting in the McpR apo form conformation.

Extended data Figure 1

A.

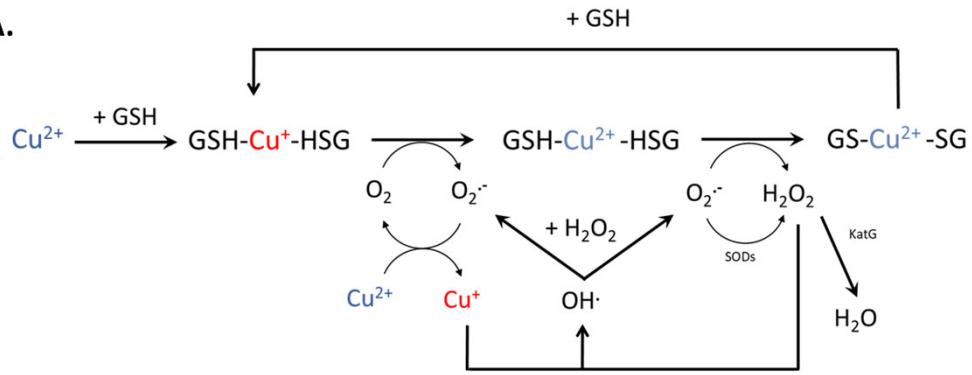

B.

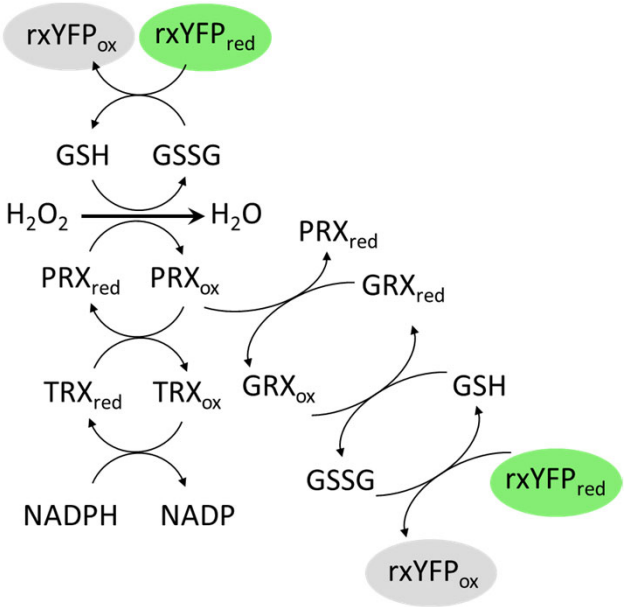

Extended data Figure 1: Potential pathways leading to ROS production by Cu. **A.** *In vitro* generation of Cu-induced ROS by Fenton-like reaction and Haber-Weiss cycles. The Cu-GSH complexes may also trigger ROS production [27,28]. The SODs and KatG are involved in $O_2^{\bullet -}$ and H_2O_2 detoxification, respectively **B.** The rxYFP biosensor is in equilibrium with the GSH pool. GSH is involved in different ways in ROS buffering. As a result, ROS production triggers an increase of the GS-SG pool, which will be partially reduced to GSH by using rxYFP as an electron donor. The resulting oxidized rxYFP will lose its fluorescence properties. GSH (glutathione), PRX (Peroxiredoxins), TRX (thioredoxin) and GRX (glutaredoxin).

Extended data Figure 2

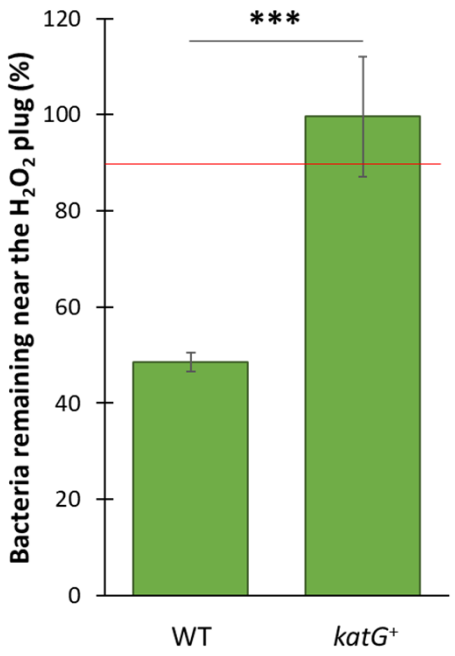

Extended data Figure 2: Overexpression of KatG prevents H_2O_2 chemotaxis. Percentage of WT and *katG*$^+$ SW cells remaining in the vicinity of the H_2O_2 plug after 25 min. An arbitrary threshold of 10% flight (corresponding to 90% of cells remaining in the vicinity of the H_2O_2 plug) is indicated in red. Mean +/- s.d., at least 3 biological replicates. *p-values* were calculated using an ANOVA (* $p < 0.05$, ** $p < 0.01$, *** $p < 0.001$).

Extended data Figure 3

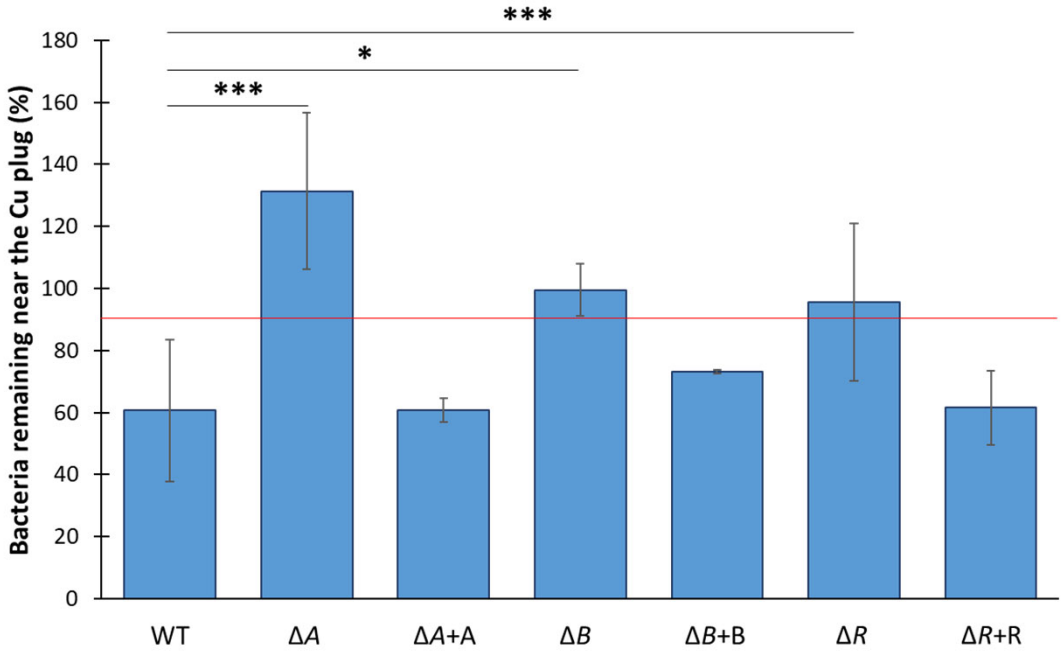

Extended data Figure 3: McpA, McpB and McpR are potentially involved in Cu chemotaxis. Percentage of WT, Δ*mcpA*, Δ*mcpA* overexpressing McpA, Δ*mcpB*, Δ*mcpB* overexpressing McpB, Δ*mcpR* and Δ*mcpR* overexpressing McpR SW cells remaining in the vicinity of the Cu plug after 25 min. An arbitrary threshold of 10% flight (corresponding to 90% of cells remaining in the vicinity of the Cu plug) is indicated in red. Mean +/- s.d., at least 3 biological replicates. *p-values* were calculated using an ANOVA (* $p < 0.05$, ** $p < 0.01$, *** $p < 0.001$).

Extended data Figure 4

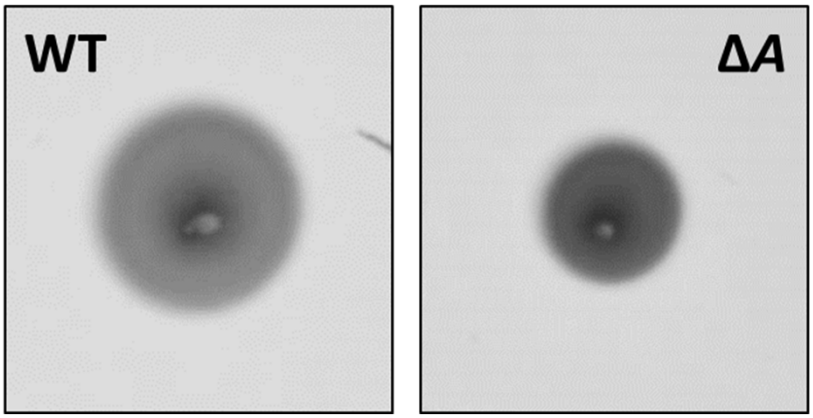

Extended data Figure 4: The Δ*mcpA* mutant is defective in chemotaxis. Chemotaxis-driven swarming pattern of the WT and Δ*mcpA* strains.

Extended data Figure 5

A.

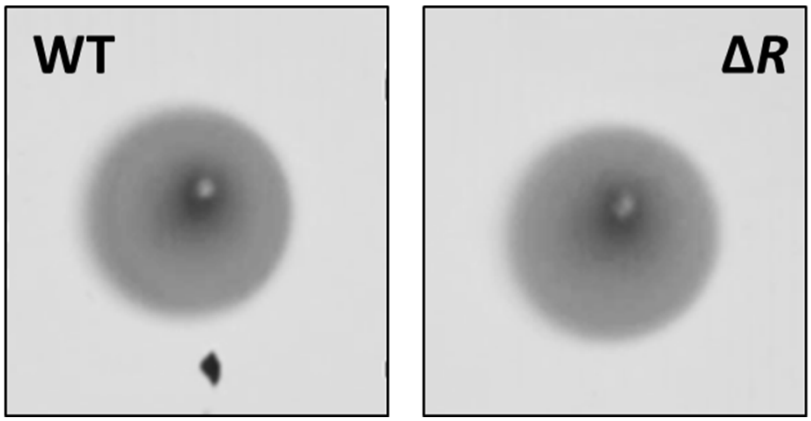

B.

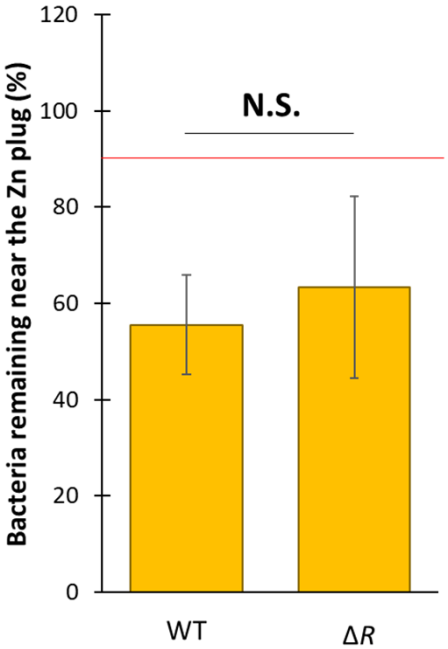

Extended data Figure 5: The chemotactic machinery is functional in the Δ*mcpR* mutant. A. Chemotaxis-driven swarming pattern of the WT and Δ*mcpR* strains. **B.** Percentage of WT and Δ*mcpR* SW cells remaining in the vicinity of the Zn plug after 25 min. An arbitrary threshold of 10% flight (corresponding to 90% of cells remaining in the vicinity of the Zn plug) is indicated in red. Mean +/- s.d., at least 3 biological replicates. *p-values* were calculated using a *t-test* (* $p < 0.05$, ** $p < 0.01$, *** $p < 0.001$).

Extended data Figure 6

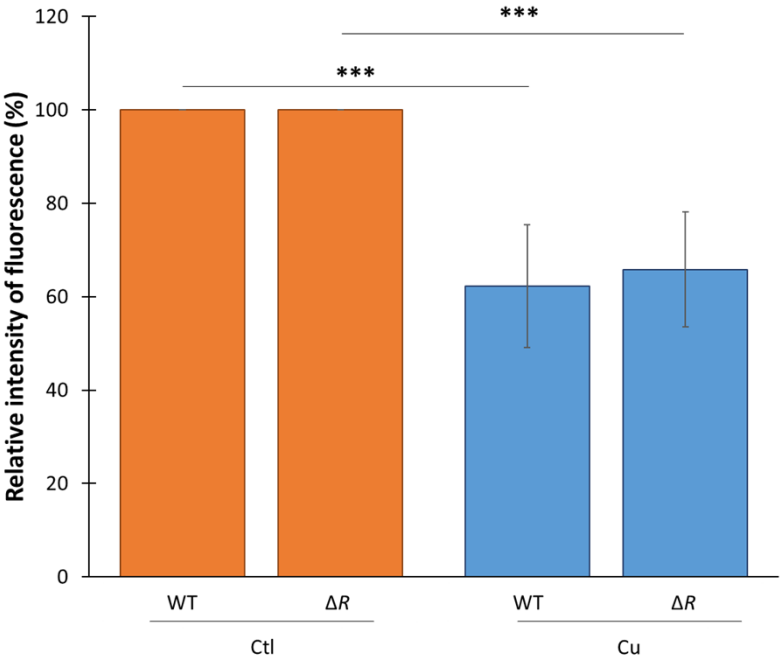

Extended data Figure 6: The Cu-induced oxidative stress is not affected in the Δ*mcpR* mutant. Relative intensity of fluorescence of the WT and Δ*mcpR* SW cells overexpressing the rxYFP biosensor and exposed to 175 µM Cu for 20 min. Mean +/- s.d., at least 3 biological replicates. *p-values* were calculated using a *t-test* (* $p < 0.05$, ** $p < 0.01$, *** $p < 0.001$).

Extended data Figure 7

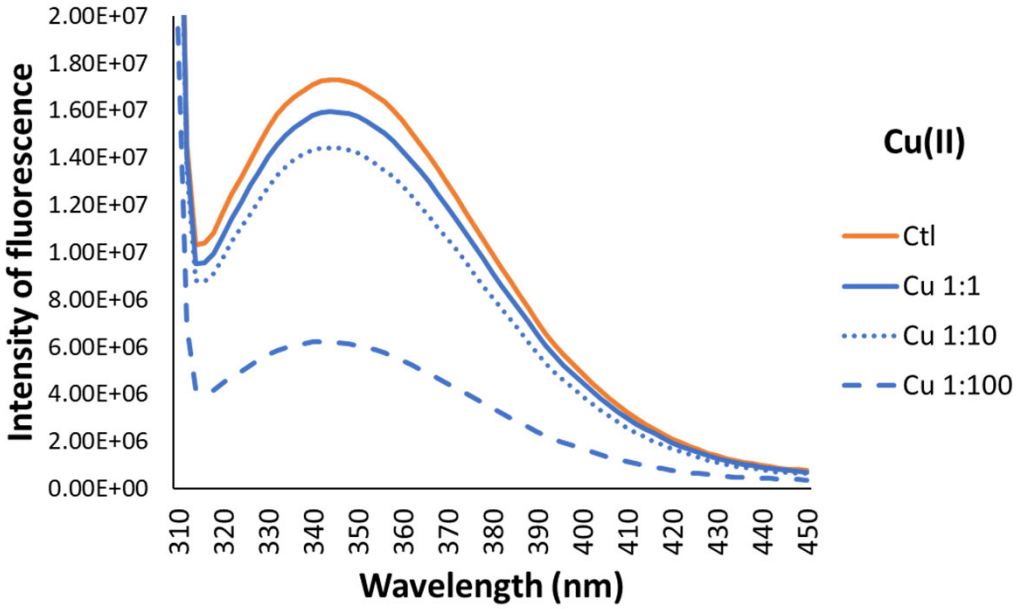

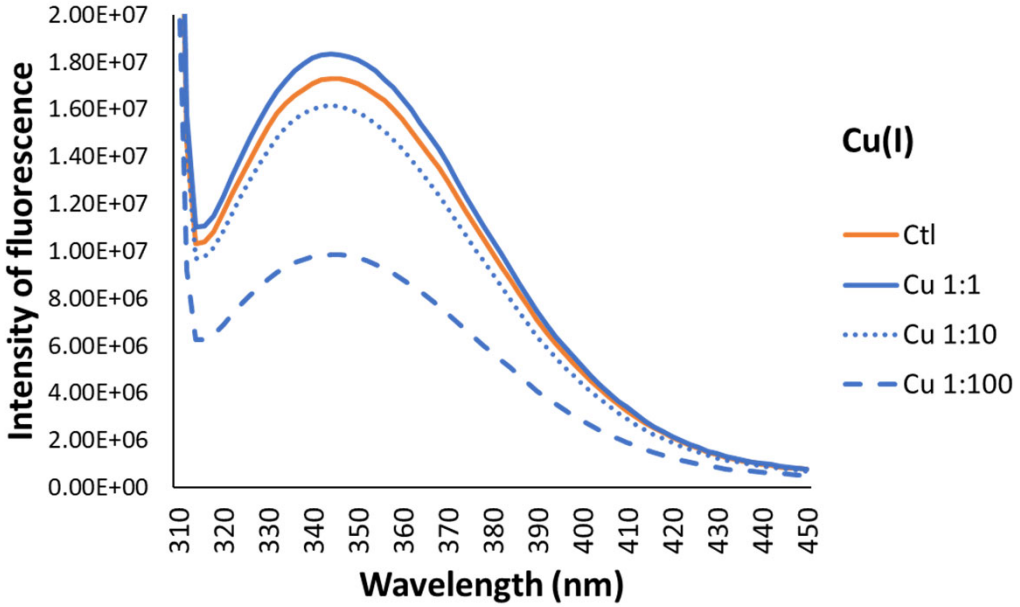

Extended data Figure 7: Representative fluorescence spectra of purified McpR. Representative intrinsic fluorescence spectra upon 280 nm excitation of purified McpR (3.58 μM) incubated with Cu(II) (top) and Cu(I) (bottom) at 1:1, 1:10 and 1:100 ratios.

Extended data Figure 8

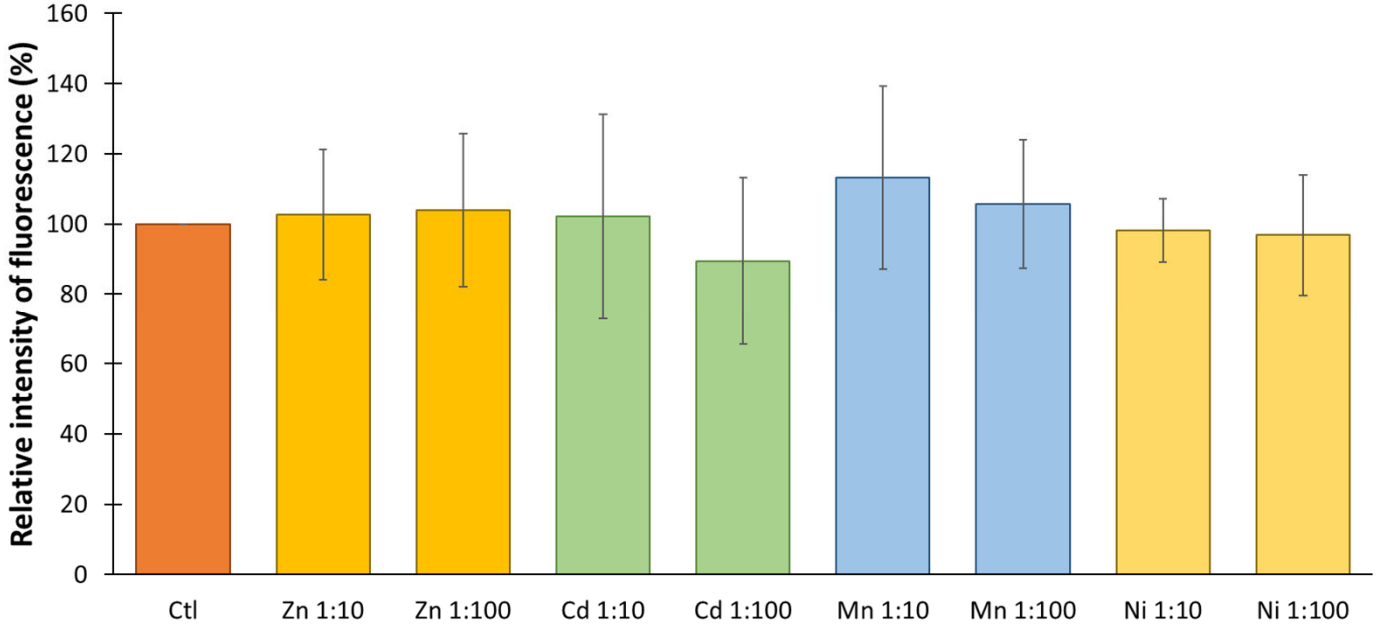

Extended data Figure 8: Zn, Cd, Mn and Ni do not directly bind to McpR. Relative intrinsic fluorescence of purified McpR (3.58 µM) incubated with $ZnSO_4$, $CdSO_4$, $MnSO_4$ and $NiSO_4$ at 1:10 and 1:100 ratios. Mean +/- s.d., at least 3 biological replicates. *p-values* were calculated using an ANOVA and were not significant ($p > 0.05$).

Extended data Figure 9

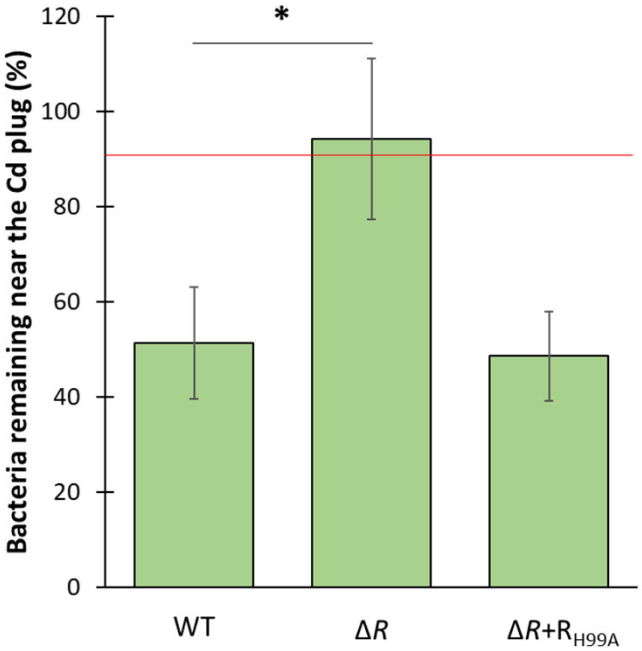

Extended data Figure 9: The $McpR_{H99A}$ mutant is still proficient for Cd chemotaxis. Percentage of WT, Δ*mcpR* and Δ*mcpR* overexpressing $McpR_{H99A}$ SW cells remaining in the vicinity of the Cd plug after 25 min. An arbitrary threshold of 10% flight (corresponding to 90% of cells remaining in the vicinity of the Cd plug) is indicated in red. Mean +/- s.d., at least 3 biological replicates. *p-values* were calculated using an ANOVA (* $p < 0.05$, ** $p < 0.01$, *** $p < 0.001$).

Extended data Figure 10

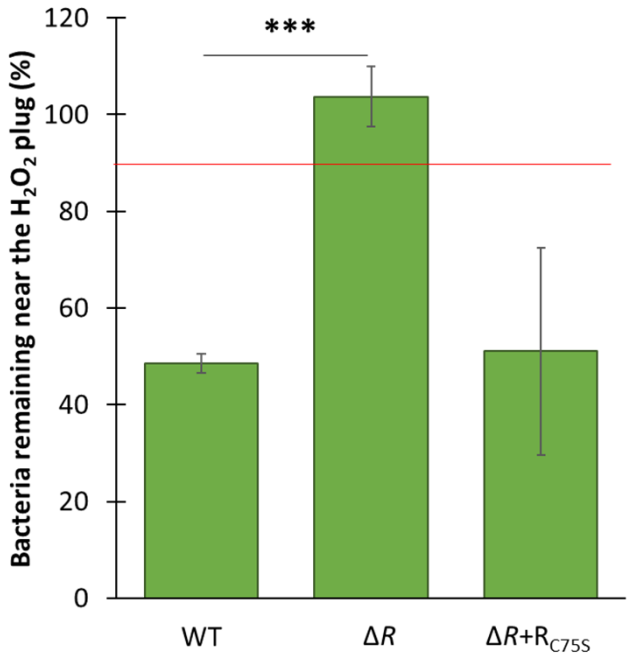

Extended data Figure 10: The $McpR_{C75S}$ mutant is still proficient for H_2O_2 chemotaxis. Percentage of WT, Δ*mcpR* and Δ*mcpR* overexpressing $McpR_{C75S}$ SW cells remaining in the vicinity of the H_2O_2 plug after 25 min. An arbitrary threshold of 10% flight (corresponding to 90% of cells remaining in the vicinity of the H_2O_2 plug) is indicated in red. Mean +/- s.d., at least 3 biological replicates, except for Δ*mcpR* overexpressing $McpR_{C75S}$ (2 biological replicates). *p-values* were calculated using an ANOVA (* $p < 0.05$, ** $p < 0.01$, *** $p < 0.001$).

Extended Data Table 1

Strains	**Relevant genotype or description**	**References**
C. crescentus		
WT	CB15N (or NA1000), synchronizable variant strain of CB15	(Evinger and Agabian, 1977)
WTrxYFP	WT strain carrying the *rxYFP* gene on the pJS14 under the control of the lac promoter; CmR	This study
ΔcheAI	Knockout strain for *cheAI* gene (CCNA_XXX)	This study
ΔA	Knockout strain for *mcpA* gene	This study
ΔA+A	Knockout strain for *mcpA* gene carrying a copy of *mcpA* on the pMR10 under the control of the lac promoter; KanR	This study
ΔB	Knockout strain for *mcpB* gene	This study
ΔB+B	Knockout strain for *mcpB* gene carrying a copy of *mcpB* on the pMR10 under the control of the lac promoter; KanR	This study
ΔC	Knockout strain for *mcpC* gene	This study
ΔD	Knockout strain for *mcpD* gene	This study
ΔE	Knockout strain for *mcpE* gene	This study
ΔF	Knockout strain for *mcpF* gene	This study
ΔG	Knockout strain for *mcpG* gene	This study
ΔH	Knockout strain for *mcpH* gene	This study
ΔI	Knockout strain for *mcpI* gene	This study
ΔJ	Knockout strain for *mcpJ* gene	This study
ΔK	Knockout strain for *mcpK* gene	This study
ΔL	Knockout strain for *mcpL* gene	This study
ΔM	Knockout strain for *mcpM* gene	This study
ΔN	Knockout strain for *mcpN* gene	This study
ΔO	Knockout strain for *mcpO* gene	This study
ΔP	Knockout strain for *mcpP* gene	This study
ΔQ	Knockout strain for *mcpQ* gene	This study
ΔR	Knockout strain for *mcpR* gene	This study
ΔRrxYFP	Knockout strain for *mcpR* gene carrying the *rxYFP* gene on the pJS14 under the control of the lac promoter; CmR	This study
ΔR+R	Knockout strain for *mcpR* gene carrying a copy of *mcpR* on the pMR10 under the control of the lac promoter; KanR	This study
ΔR+RH99A	Knockout strain for *mcpR* gene carrying a copy of *mcpR* with the mutation H99A on the pMR10 under the control of the lac promoter; KanR	This study
ΔR+RC75S	Knockout strain for *mcpR* gene carrying a copy of *mcpR* with the mutation C75S on the pMR10 under the control of the lac promoter; KanR	This study
ΔS	Knockout strain for *mcpS* gene	This study
sodB+	WT strain carrying a copy of *sodB* on the pMR10 under the control of the lac promoter; KanR	This study
katG+	WT strain carrying a copy of *katG* on the pMR10 under the control of the lac promoter; KanR	This study
WTrxYFP	WT strain carrying the *rxYFP* gene on the pJS14 under the control of the lac promoter; CmR	This study
E. coli		
S17-1	RP4-2, Tc::Mu, KM-Tn7, for plasmid mobilization	
BL21	BL21 *E. coli* strain used for overexpression of proteins	
Plasmids	**Relevant genotype or description**	
pNPTS138	mobRP4+ ori-R6K sacB; integrative vector in *C. crescentus* for in-frame deletions; KanR	
pMR10	DH10B strain carrying the pMR10 low copy number replicative cloning vector in *E. coli* and *C. crescentus* ; KanR	
pJS14	DH10B strain carrying the pJS14 medium copy number replicative cloning vector in *E. coli* and *C. crescentus* ; CmR	
pET28a	BL21 strain carrying the pET28a high copy number replicative cloning vector in *E. coli* ; KanR	

Extended Data Table 1: Strains and plasmids

Supplementary information

Caulobacter crescentus genome is predicted to encode two chemotaxis clusters including genes coding for CheA histidines kinases, CheY response regulators, CheW adaptors, CheB methylesterases, CheR methytransferases, McpA and McpK and other uncharacterized Che proteins. Most of the studies conducted in *C. crescentus* so far focused on the major chemotaxis cluster (cluster 1) [1-4] while the second alternate chemotaxis cluster (cluster 2) was only recently investigated[5]. These studies concluded that the cluster 1 is essential for chemotaxis, while cluster 1 and cluster 2 are involved in biofilm formation and holdfast production[3,5]. Consistent with these observations, CheAI (cluster 1 CheA) turns out to be the main histidine kinase involved in chemotaxis while the exact function of CheAII (cluster 2 CheA) remains unknown[5]. In order to determine which CheA is involved in Cu-chemotaxis, we constructed the Δ*cheAI*, Δ*cheAII* and Δ*cheAI-II* mutants and assessed their chemotactic behavior to Cu by LCI (**Fig. 1**). The Δ*cheAI* mutant completely lost its chemotactic response to Cu, while the Δ*cheAII* mutant displayed a WT phenotype. Accordingly, the Δ*cheAI-II* double mutant showed a similar behavior to the Δ*cheAI* mutant. These data confirm that the CheAI histidine kinase is the main histidine kinase involved in Cu chemotaxis.

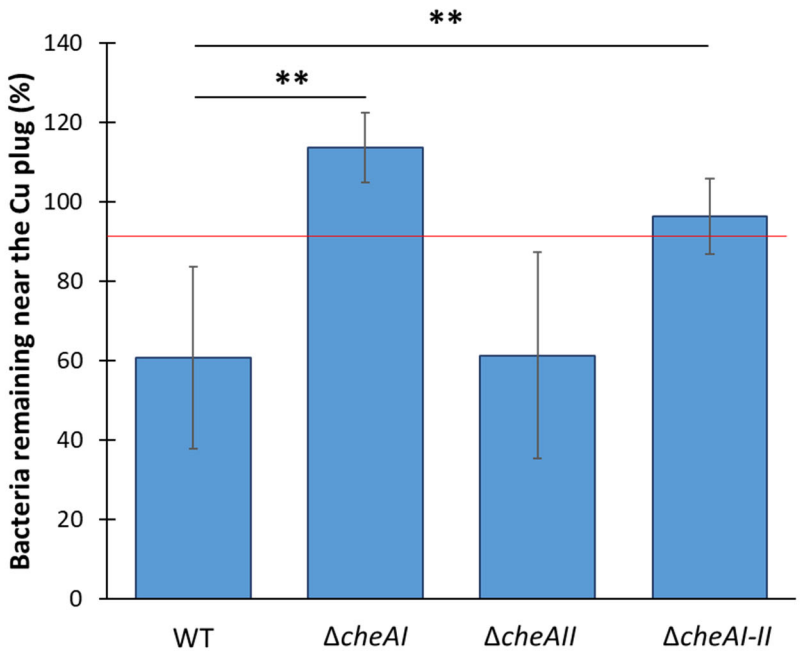

Figure 1: CheAI is the main histidine kinase involved in Cu chemotaxis. Percentage of WT, Δ*cheAI*, Δ*cheAII* and Δ*cheAI-II* SW cells remaining in the vicinity of the Cu plug after 25 min. An arbitrary threshold of 10% flight (corresponding to 90% of cells remaining in the vicinity of the Cu plug) is indicated in red. Mean +/- s.d., at least 3 biological replicates. *p-values* were calculated using an ANOVA (* $p < 0.05$, ** $p < 0.01$, *** $p < 0.001$).

Bibliography

1 Alley, M. R., Maddock, J. R. & Shapiro, L. Polar localization of a bacterial chemoreceptor. *Genes Dev* **6**, 825-836, doi:10.1101/gad.6.5.825 (1992).

2 Alley, M. R., Maddock, J. R. & Shapiro, L. Requirement of the carboxyl terminus of a bacterial chemoreceptor for its targeted proteolysis. *Science* **259**, 1754-1757, doi:10.1126/science.8456303 (1993).

3 Tsai, J. W. & Alley, M. R. Proteolysis of the McpA chemoreceptor does not require the *Caulobacter* major chemotaxis operon. *J Bacteriol* **182**, 504-507, doi:10.1128/JB.182.2.504-507.2000 (2000).

4 Tsai, J. W. & Alley, M. R. Proteolysis of the *Caulobacter* McpA chemoreceptor is cell cycle regulated by a ClpX-dependent pathway. *J Bacteriol* **183**, 5001-5007, doi:10.1128/JB.183.17.5001-5007.2001 (2001).

5 Berne, C. & Brun, Y. V. The Two Chemotaxis Clusters in *Caulobacter crescentus* Play Different Roles in Chemotaxis and Biofilm Regulation. *J Bacteriol* **201**, doi:10.1128/JB.00071-19 (2019).